Design and Simulation of a Wideband Wire Antenna Generated from Control Points of a Curve Projected from a Lemniscatic Torus for 5G Applications

Daniel A. Flores-Córdova*, Carlos E. Arellano-Ramírez, Ricardo Velezmoro-León and Robert Ipanaqué-Chero

Universidad Nacional de Piura, Piura, Peru

Abstract

Wideband, compact, and low-cost radiating elements are a bottleneck in the densification of 5G base stations in the n78 band, yet most published designs still arrive at their geometry by perturbing a canonical shape — a patch, a monopole, a slot - through trial and error. Such a process is hard to document, hard for a third party to reproduce exactly, and offers no systematic route to neighbouring geometries. This paper asks instead whether a radiating shape can be derived in closed form from differential geometry. We generate a wire antenna from control points sampled on the planar projection of a curve lying on a lemniscatic torus: the entire layout follows from two coprime integer parameters and is produced symbolically in the Wolfram Language, so that any reader can regenerate the exact geometry from the published expressions. The resulting 103 mm × 100 mm element was simulated with the free solver 4NEC2 and cross-validated against a three-dimensional full-wave solver; both place its natural impedance minimum inside the 3400–3600 MHz 5G band. Matched to 50 Ω by a two-component high-pass L network, the element attains SWR $\leq$ 1.28 and a reflection coefficient below -18 dB across that band, and holds SWR $\leq$ 1.6 from approximately 3200 MHz to 3625 MHz, a 12.5% impedance bandwidth that covers the whole of its 3400–3600 MHz design band. With a sectorial pattern and 3.29 dBi gain it is consistent with the requirements of base-station panel elements. The contribution is less the particular antenna than the design route: a parameter-driven family of geometries in which bandwidth and pattern are explored by changing two integers rather than by manual reshaping.

Keywords

Lemniscatic torus, Parametric curves, Wire antenna, 5G n78, Reproducible antenna design, Symbolic computation, 4NEC2, Impedance matching, SWR

1. Introduction

The densification of fifth-generation (5G) networks in the sub-6 GHz spectrum has concentrated a large share of worldwide deployment in the n78 band (3.3–3.8 GHz), where operators need radiating elements that are simultaneously wideband, physically compact, and cheap enough to be replicated many times over in base-station panel arrays. An antenna is the transitional structure between free space and a guiding device [1], and the quality of that transition governs how much of the delivered power actually leaves the array [2]; achieving it across several hundred megahertz without resorting to multi-layer stacks or multi-port feeding networks remains a practical design problem.

Recent sub-6 GHz proposals illustrate both the progress and the cost of the prevailing approach. π-shaped monopole arrays cover 3.3-6.0 GHz for indoor base stations, but require a sixteen-port arrangement [3]; four-element monopole-based MIMO antennas reach 2.88–6.12 GHz through a multi-element configuration [4]; and the massive-MIMO architectures surveyed in [5] trade bandwidth against substantial feed-network complexity. What these designs share is their genesis: a canonical geometry subsequently perturbed by trial and error until the desired response appears. That route is effective, but

IWSAI 2026: 1st International Workshop on Systems, Applications, Artificial Intelligence and Innovation, September 16–18, 2026, Piura, Peru

*Corresponding author.
dflores@unp.edu.pe (D. A. Flores-Córdova); carellanor@unp.edu.pe (C. E. Arellano-Ramírez); rvelezmorol@unp.edu.pe (R. Velezmoro-León); ripanaquec@unp.edu.pe (R. Ipanaqué-Chero)
0000-0001-8022-1900 (D. A. Flores-Córdova); 0000-0002-6115-1801 (C. E. Arellano-Ramírez); 0000-0002-2582-8264 (R. Velezmoro-León); 0000-0002-3873-6780 (R. Ipanaqué-Chero)

CEUR Workshop Proceedings ceur-ws.org ISSN 1613-0073
published 2026-09-14

it is difficult to document, difficult to reproduce exactly, and it provides no systematic way of asking what a neighbouring geometry would have done.

This work explores the opposite starting point: rather than perturbing a shape until it radiates as required, we derive the shape in closed form from the differential geometry of a surface. Symbolic computation makes this practical, since complex geometries such as tori built from arbitrary profile curves can be described exactly and manipulated with ease [6], and the use of such software for modelling and simulating physical structures is by now well established [7]. The advantage is not aesthetic. Because the layout is the image of a small set of analytic expressions, it is fully specified by a handful of parameters, it can be regenerated exactly by any reader, and neighbouring geometries can be enumerated by changing those parameters rather than by redrawing.

The approach builds on our earlier demonstration that antenna layouts can be generated symbolically in Mathematica and analysed in 4NEC2 [8], which established the design flow for antennas in the 2100 and 3500 MHz bands. The present work extends it in three directions: the generating surface is a lemniscatic torus rather than a torus of revolution, the choice of generating parameters is given an explicit criterion, and the resulting element is cross-validated against a three-dimensional full-wave solver. The particular geometry analysed here, together with the 4NEC2 results of Sections 4.1 to 4.4, was obtained in the undergraduate thesis [9] carried out at our institution under the supervision of two of the present authors; Sections 3.1, 4.5 and 5.1 are new to this paper.

Concretely, we take a curve lying on a lemniscatic torus [6], project it onto the XY plane, and sample control points from that projection to define a planar wire antenna. The geometry is generated in the Wolfram Language [10] of the Mathematica symbolic computation system [11] and simulated with the free electromagnetic solver 4NEC2 [12], built on the NEC-2 method-of-moments kernel [13]; the model is additionally cross-validated against a three-dimensional full-wave solver [14]. Both solvers place the natural impedance minimum of the resulting 103 mm × 100 mm element inside the 3400–3600 MHz band.

The main contributions of this work are: (i) an analytical, fully symbolic procedure that generates planar antenna geometries from curves on a lemniscatic torus, in which the complete layout is determined by two coprime integer parameters, together with an explicit criterion for selecting them; (ii) a concrete 10.5 cm × 10.5 cm single-element realisation which, matched by a two-component high-pass L network, covers the n78 5G band; (iii) a cross-validation of the NEC-2 wire model against a three-dimensional full-wave solver, which bounds the confidence that can be placed in the reported impedance values; and (iv) a design flow relying exclusively on widely available software, with the complete geometry released openly, so that every result reported here can be reproduced independently.

The remainder of the paper is organized as follows. Section 2 presents the mathematical preliminaries. Section 3 describes the generation of the antenna geometry in the Wolfram Language and justifies the choice of parameter functions. Section 4 reports the implementation and simulation results obtained with 4NEC2, before and after impedance matching, together with the full-wave cross-validation. Section 5 discusses the results in the context of recent sub-6 GHz antenna designs and of a printed-circuit realisation, and Section 6 states the conclusions.

2. Mathematical Preliminaries

2.1. Surfaces of revolution

Let C be a curve lying in a plane $P \subset \mathbb{R}^3$ and let A be a straight line also contained in P that does not intersect C. When the profile curve C rotates about the line A, it generates a surface of revolution [15].

2.2. Torus of revolution

The torus of revolution is the surface of revolution obtained when the profile curve C is a circle, according to Subsection 2.1 [16].

2.3. Lemniscate of Bernoulli

The lemniscate of Bernoulli is defined as the locus of points in a plane such that the product of their distances to two fixed points of the same plane, (-A, 0) and (A, 0), with $A > 0$, is a constant A^2. The Cartesian equation obtained from this definition is $(x^2 + y^2)^2 = 2A^2(x^2 + y^2)$. The parametric equations for the lemniscate with half-width A are [17].

$$x(t) = \frac{Acos(t)}{1 + sen^2(t)}, \quad y(t) = \frac{Acos(t)sen(t)}{1 + sen^2(t)}, \quad 0 < t < 2\pi \tag{1}$$

2.4. The lemniscatic torus

For the generation of the lemniscatic torus, it must be noted that the profile curve and the axis of rotation do not lie in the same plane, as shown in Figure 1. The parametric equations of a lemniscate of Bernoulli contained in the plane $x = B$, $B \in \mathbb{R}$, are

$$x(v) = B, \quad y(v) = \frac{Acos(v)}{1 + sen^2(v)}, \quad z(v) = \frac{Acos(v)sen(v)}{1 + sen^2(v)}, \quad -\frac{\pi}{2} < v < \frac{\pi}{2} \tag{2}$$

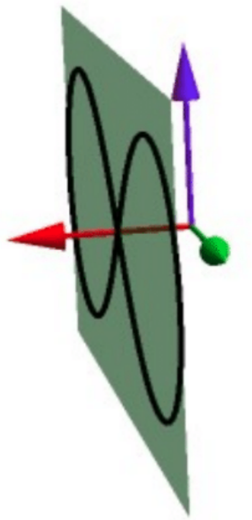

Figure 1: Arrangement of the lemniscate that rotates about the Z axis.

Given the rotation matrix

$$R(u) = \begin{pmatrix} cos(u) & -sen(u) & 0 \\ sen(u) & cos(u) & 0 \\ 0 & 0 & 1 \end{pmatrix} \tag{3}$$

the lemniscatic torus (Figure 2) is defined by $LT(u, v) = R(u)(x(v), y(v), z(v))^T$, where $0 < u < 2\pi$ and $-\frac{\pi}{2} < v < \frac{\pi}{2}$. Explicitly,

$$LT(u, v) = (B\ cos(u) - \frac{Acos(u)sen(v)}{1 + sen^2(v)}, \quad B\ sen(u) + \frac{Acos(u)cos(v)}{1 + sen^2(v)}, \quad \frac{Asen(v)cos(v)}{1 + sen^2(v)}) \tag{4}$$

With the Mathematica software we define it as:

```
LT[{u_,v_},{A_,B_}]:={B Cos[u]-(A Cos[v] Sin[u])/(1+Sin[v]^2),
B Sin[u]+(A Cos[u] Cos[v])/(1+Sin[v]^2),(A Cos[v] Sin[v])/(1+Sin[v]^2)}
```

For the purpose of the antenna design we explicitly evaluate the lemniscatic torus at $A = 1$ and $B = \frac{1}{4}$, i.e., $LT[\{u, v\}, \{1, \frac{1}{4}\}]$, obtaining

$$\frac{cos(u)}{4} - \frac{cos(v)sen(u)}{1 + sen^2(v)}, \quad \frac{sen(u)}{4} + \frac{cos(u)cos(v)}{1 + sen^2(v)}, \quad \frac{cos(v)sen(v)}{1 + sen^2(v)}) \tag{5}$$

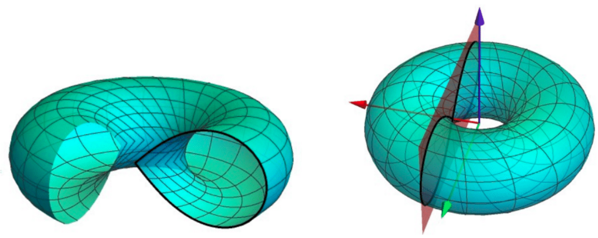

Figure 2: The profile curve generates the torus (left); the lemniscate in the plane and the generated torus (right).

The basic families of curves inherent to the lemniscatic torus are parallel circumferences, while the meridians are lemniscate arcs.

2.5. Curves on a lemniscatic torus

Curves lying on the lemniscatic torus are obtained by substituting the parameters u and v with differentiable functions $a_1(t)$ and $a_2(t)$, respectively; that is, $CLT(a_1(t), a_2(t))$. With the software this is defined by:

```
CLT[t_,a:{_,_},{A_,B_}]:=Module[{uu,vv},LT[{uu,vv},{A,B}]/.{uu>a[[1]],
vv->a[[2]]}]
```

The local binding of the surface parameters is deliberate: defining CLT in terms of the global symbols u and v, as is sometimes done, makes the result silently incorrect for any reader whose session already assigns those names.

For the case at hand (Figure 3) we define $Cur1[t] := CLT[t, \{3t, 7t\}, \{1, \frac{1}{4}\}]$ and obtain the following curve equation 6:

$$\frac{cos(3t)}{4} - \frac{cos(7t)sen(3t)}{1 + sen^2(7t)}, \quad \frac{sen(3t)}{4} + \frac{cos(3t)cos(7t)}{1 + sen^2(7t)}, \quad \frac{cos(7t)sen(7t)}{1 + sen^2(7t)}) \tag{6}$$

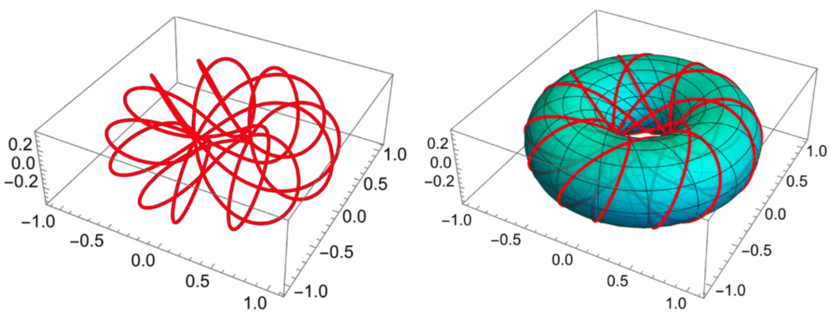

Figure 3: The curve Cur1[t] alone (left) and together with the lemniscatic torus (right).

3. Antenna Design with the Wolfram Language

Having defined the lemniscatic torus and the parametric curves intrinsic to it, we project the curve onto the XY plane by eliminating the third component of $CLT[t, a, \{A, B\}]$. To simplify subsequent calculations, we define the planar curve Curv as follows:

```
Curv[t_]:=Delete[Cur1[t],-1]
```

and we obtain the following plane curve, shown in Figure 4:

$$\left(\frac{cos(3t)}{4} - \frac{cos(7t)sen(3t)}{1+sen^2(7t)}, \quad \frac{sen(3t)}{4} + \frac{cos(3t)cos(7t)}{1+sen^2(7t)}\right) \tag{7}$$

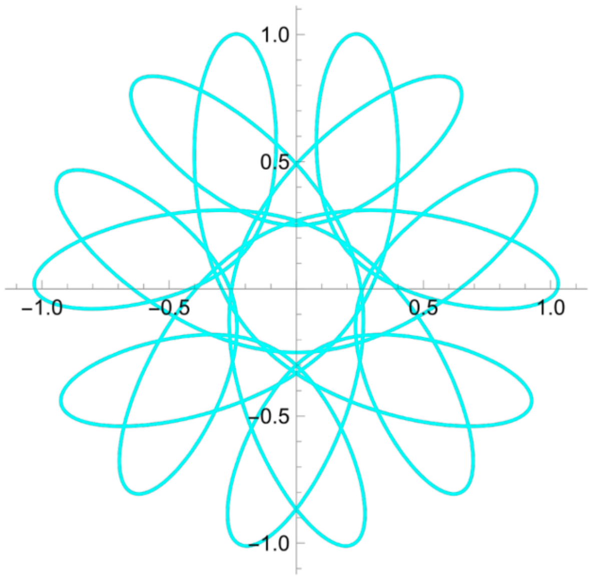

Figure 4: The projected planar curve Curv[t].

The domain of the curve is the interval $[0, 2\pi]$. This segment is partitioned into subsegments of equal length $\frac{\pi}{84}$, and the following values of the parameter t are selected, in the order given below:

```
l1=Pi {143/84,12/7,145/84,55/42,73/42,7/4,37/28,23/21,23/12,17/14,
  43/84,2/3,31/28,19/28,29/42,47/42,59/84,5/7,61/84};
```

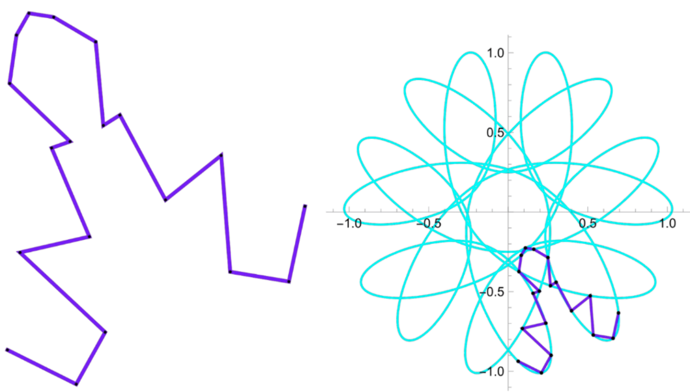

Figure 5: Control points of the base pattern (left) and a partial antenna layout (right).

Next, we find the points that determine a base pattern (Figure 5) by applying Curv to each element of l1:

```
pl1=N[Curv/@l1,4];
```

Table 1
Values of the parameter t and the corresponding control points of the base pattern pl1.

$t(\times\pi)$	**Control point** (x, y)	$t(\times\pi)$	**Control point (x, y)**
143/84	(0.0630, -0.9371)	43/84	(0.1610, -0.2334)
12/7	(0.2086, -1.0090)	2/3	(0.2500, -0.2857)
145/84	(0.2699, -0.8995)	31/28	(0.2661, -0.4625)
55/42	(0.0896, -0.7311)	19/28	(0.3012, -0.4404)
73/42	(0.2365, -0.6975)	29/42	(0.5157, -0.5258)
37/28	(0.1956, -0.4964)	59/84	(0.5350, -0.7719)
23/21	(0.0675, -0.3736)	5/7	(0.6591, -0.7925)
23/12	(0.0821, -0.2714)	61/84	(0.6933, -0.6335)
17/14	(0.1084, -0.2252)		

The complete list of 133 control points that determines the antenna geometry is generated by applying appropriate rotations to the base pattern of Table 1, which was obtained in [9]. Figure 5 shows the control points together with a portion of the design, and Figure 6 shows the resulting antenna geometry. The full coordinate list, the Mathematica notebook that generates it and the 4NEC2 input file are openly available; see the Data and code availability statement.

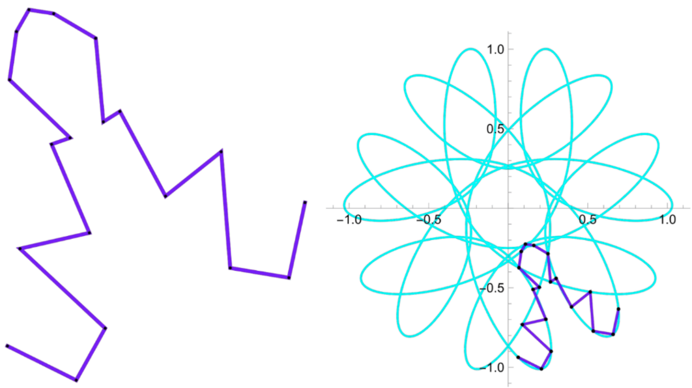

Figure 6: The antenna geometry alone (left) and together with the curve Curv[t] (right).

3.1. Choice of the parameter functions

The curve on the lemniscatic torus is obtained by substituting the surface parameters with differentiable functions, $CLT(a_1(t), a_2(t))$. Throughout this work we restrict attention to the linear family $a_1(t) = pt$ and $a_2(t) = qt$ with p, q positive integers, which is the smallest family that produces closed, non-degenerate projections. Three conditions govern the choice of the pair (p, q). First, closure: the projected curve closes on $t \in [0, 2\pi]$ and is traced exactly once if and only if p and q are coprime, since non-coprime pairs retrace a sub-curve and yield duplicated control points. Second, symmetry: the integer q fixes the number of lemniscatic oscillations per revolution and therefore imposes a q-fold rotational symmetry on the projection, while p governs the winding of the curve about the axis of revolution. Third, developed length: for a fixed outer dimension, larger q densifies the layout and increases the developed length of the resulting wire, which in turn increases the number of natural resonances falling within a given frequency span.

A convenient closed form makes the role of each parameter explicit. Carrying out the rotation of equation (4) and deleting the third component, the projected curve reduces to a pure rotation at angular rate p applied to a radial profile oscillating at rate q, $Curv_{p,q}(t) = R(pt)(\frac{B,\ Acos(qt)}{1+sen^2(qt)})^T$, from which two consequences follow at once. The substitution $t \to t + \frac{2\pi}{q}$ leaves the radial profile invariant and rotates the point by $\frac{2\pi p}{q}$; since p and q are coprime these rotations generate the cyclic group of order q, which is the origin of the q-fold symmetry noted above. And it is the ratio $\frac{p}{q}$, rather than either integer alone, that governs how uniformly a given partition of the parameter domain samples the curve.

For the antenna reported here we adopt $(p, q) = (3, 7)$. The 7-fold symmetry induced by $a_2(t) = 7t$ is directly visible in the final layout: the base pattern of Table 1 comprises 19 control points, and the complete geometry is the union of seven copies of that pattern rotated by $\frac{2\pi}{7}$, giving $719 = 133$ control points. The nineteen parameter values listed in (7) are themselves structured: partitioning $[0, 2\pi]$ into 168 subintervals of length $\frac{\pi}{84}$ places 24 candidate values in each $\frac{2\pi}{7}$ sector, of which 19 are retained and 5 discarded. The resulting layout occupies 103.1 mm × 100.5 mm and its developed wire length is 930 mm, that is 10.85 λ at 3.5 GHz — a strongly multi-resonant structure whose closely spaced natural resonances overlap and smooth the frequency variation of its input impedance. This is the physical mechanism behind the wideband behaviour reported in Section 4.

Table 2 reports the low-order coprime pairs examined, all normalised to the same 103 mm outer dimension. The geometric figures of merit already discriminate sharply between candidates: three pairs - $(2, 5)$, $(3, 7)$ and $(4, 9)$, all with p/q close to 0.43 - yield compact, evenly sampled layouts whose longest chord stays between 12.3 mm and 16.6 mm, while every other pair produces chords of 34 mm to 96 mm, that is, tangled outlines with long jumps that are both poor radiators and badly conditioned for a segmented numerical model. Among the three, $(3, 7)$ minimises the longest chord, and this is the criterion that led to its adoption. We note that the sampling pattern of (7) was curated for $(3, 7)$, so the remaining pairs are somewhat penalised by reusing it rescaled; a dedicated selection for each pair would be required for a fully impartial comparison.

Table 2
Low-order coprime pairs (p, q) and the resulting geometry, normalised to a 103 mm outer dimension.

(p, q)	$\frac{p}{q}$	Control points	Outer size (mm)	Developed length (mm)	$\frac{L}{\lambda}$ at 3.5 GHz	Longest chord (mm)
(1, 3)	0.333	57	103.1 × 89.6	1071	12.50	34.1
(2, 5)	0.400	95	98.0 × 103.1	765	8.92	13.5
(3, 5)	0.600	95	103.1 × 98.0	3047	35.55	81.9
(2, 7)	0.286	133	100.5 × 103.1	3676	42.88	95.4
(3, 7)	0.429	133	103.1 × 100.5	930	10.85	12.3
(4, 7)	0.571	133	100.5 × 103.1	4042	47.16	95.8
(5, 7)	0.714	133	103.1 × 100.5	4434	51.73	82.5
(3, 8)	0.375	152	103.1 × 103.1	2051	23.93	50.7
(4, 9)	0.444	171	101.5 × 103.1	1457	17.00	16.6

4. Implementation and Simulation with 4NEC2

4.1. Implementation of the antenna model

The control points of Table 1 (extended by rotation to the complete set) were entered into the 4NEC2 software; a spreadsheet was used to organize the coordinate input, as shown in Figure 7. Once all control points were entered, 4NEC2 rendered the antenna model, whose overall dimensions are approximately 10.5 cm × 10.5 cm (Figure 8). This compact size makes the antenna suitable for fabrication on printed circuit boards (PCB) and for integration into antenna arrays such as the panel antennas used in 5G cellular base stations.

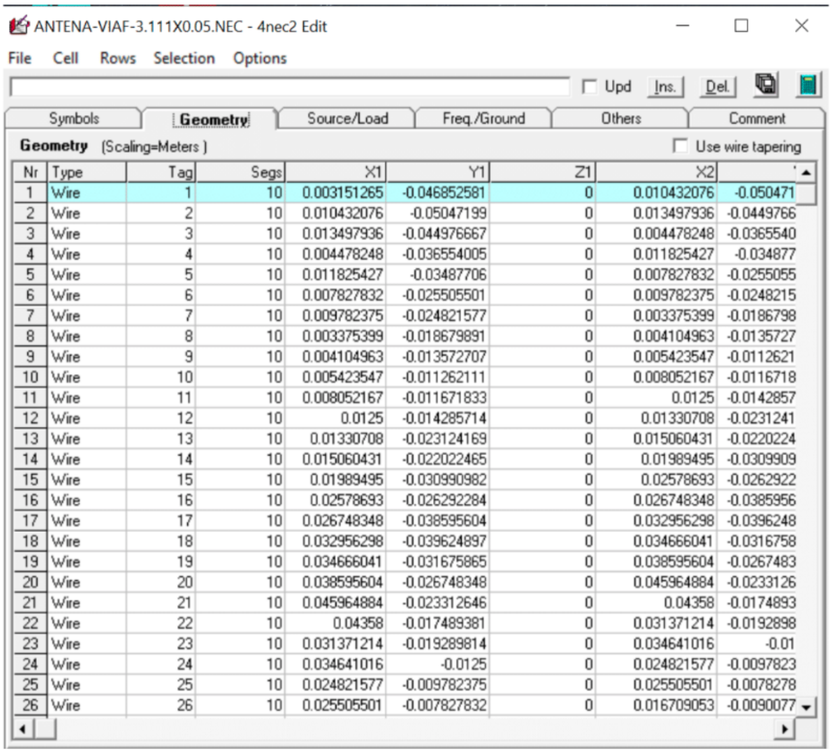

Nr	Type	Tag	Segs	X1	Y1	Z1	X2	
1	Wire	1	10	0.003151265	-0.046852581	0	0.010432076	-0.050471
2	Wire	2	10	0.010432076	-0.05047199	0	0.013497936	-0.0449766
3	Wire	3	10	0.013497936	-0.044976667	0	0.004478248	-0.0365540
4	Wire	4	10	0.004478248	-0.036554005	0	0.011825427	-0.034877
5	Wire	5	10	0.011825427	-0.03487706	0	0.007827832	-0.0255055
6	Wire	6	10	0.007827832	-0.025505501	0	0.009782375	-0.0248215
7	Wire	7	10	0.009782375	-0.024821577	0	0.003375399	-0.0186798
8	Wire	8	10	0.003375399	-0.018679891	0	0.004104963	-0.0135727
9	Wire	9	10	0.004104963	-0.013572707	0	0.005423547	-0.0112621
10	Wire	10	10	0.005423547	-0.011262111	0	0.008052167	-0.0116718
11	Wire	11	10	0.008052167	-0.011671833	0	0.0125	-0.0142857
12	Wire	12	10	0.0125	-0.014285714	0	0.01330708	-0.0231241
13	Wire	13	10	0.01330708	-0.023124169	0	0.015060431	-0.0220224
14	Wire	14	10	0.015060431	-0.022022465	0	0.01989495	-0.0309909
15	Wire	15	10	0.01989495	-0.030990982	0	0.02578693	-0.0262922
16	Wire	16	10	0.02578693	-0.026292284	0	0.026748348	-0.0385956
17	Wire	17	10	0.026748348	-0.038595604	0	0.032956298	-0.0396248
18	Wire	18	10	0.032956298	-0.039624897	0	0.034666041	-0.0316758
19	Wire	19	10	0.034666041	-0.031675865	0	0.038595604	-0.0267483
20	Wire	20	10	0.038595604	-0.026748348	0	0.045964884	-0.0233126
21	Wire	21	10	0.045964884	-0.023312646	0	0.04358	-0.0174893
22	Wire	22	10	0.04358	-0.017489381	0	0.031371214	-0.0192898
23	Wire	23	10	0.031371214	-0.019289814	0	0.034641016	-0.01
24	Wire	24	10	0.034641016	-0.0125	0	0.024821577	-0.0097823
25	Wire	25	10	0.024821577	-0.009782375	0	0.025505501	-0.0078278
26	Wire	26	10	0.025505501	-0.007827832	0	0.016709053	-0.0090077

Figure 7: Entry of the control points into the 4NEC2 software.

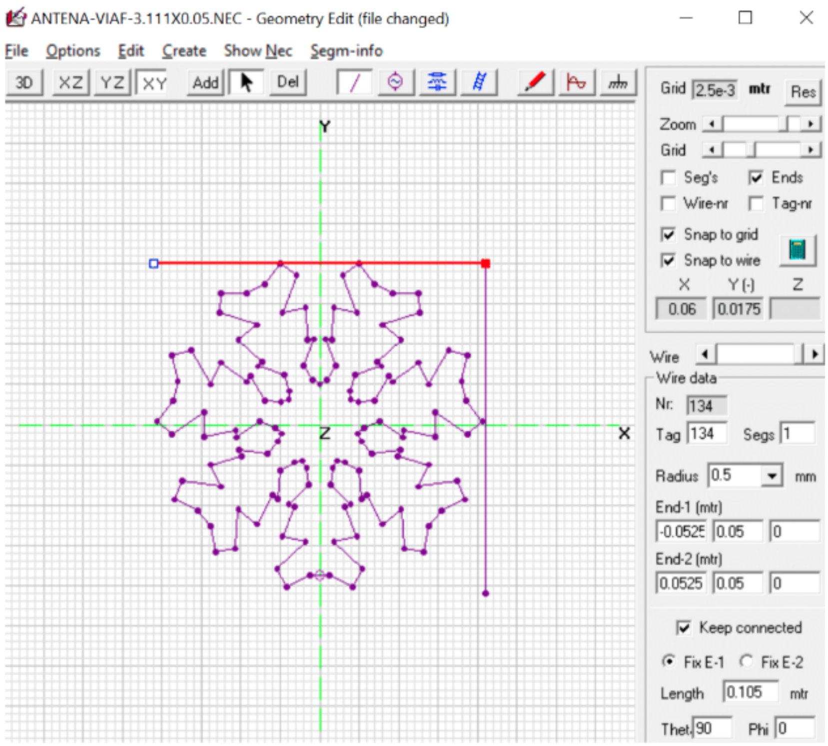

Figure 8: Overall dimensions of the antenna (length × width).

4.1.1. Numerical model and its validity limits

The antenna was modelled in 4NEC2 as a closed polyline of 133 straight wire sections joining the control points, with a uniform conductor radius $a = 0.5$ mm. Each section was subdivided into ten segments, giving 1329 segments in total for a developed wire length of 930 mm, so that the mean segment length is $\Delta = 0.70$ mm and the longest is 1.23 mm. The model was run with the extended thin-wire kernel and in free space. The kernel is accurate provided the segment length remains small with respect to the wavelength and large with respect to the conductor radius [13]. The first condition is comfortably met: at the highest simulated frequency, 3700 MHz ($\lambda = 81.1$ mm), the longest segment is $\frac{\lambda}{66}$ and $\frac{a}{\lambda} = 0.0062$, both well inside the customary limits.

The second condition is not. With ten segments per section the ratio $\frac{\Delta}{a}$ is 1.40 on average and never exceeds 2.47, which places the discretisation below the range in which even the extended kernel is reliable. Table 3 reports the sensitivity of the computed input impedance to this choice. Coarsening the mesh until $\frac{\Delta}{a}$ exceeds 2 moves the reactance from -153 Ω to between -120 Ω and -77 Ω while the resistance stays within 245-273 Ω, so that the unmatched SWR at 3500 MHz falls from 7.09 to approximately 5.8. We report this openly: the absolute input impedance of the present model carries an uncertainty of the order of 25%, and the value obtained with the finest mesh is the least reliable of the set. The better-conditioned meshes move towards the value returned by the independent full-wave model of Section 4.5, which gives an unmatched SWR of 5.00.

The engineering conclusion is nevertheless robust against this uncertainty. Repeating the design on the best-conditioned mesh ($\frac{\Delta}{a} = 3.50$) yields an optimum matching network of 0.414 pF and 5.05 nH, against 0.37 pF and 5.27 nH for the mesh used here, and an impedance bandwidth of 12.9% against 12.5%. The component values shift by about a tenth and the bandwidth is essentially unchanged: what the discretisation affects is the absolute impedance, not the conclusion that a two-component network covers the design band.

The conductor was modelled as a perfect electric conductor, so that the structure loss reported by the solver is zero and the radiation efficiency is 100% by construction; the ohmic loss of a real copper conductor is therefore not included in the figures below. The structure was analysed in free space, without a dielectric substrate, a ground plane or a feeding connector; the consequences of these simplifications are discussed in Section 5.

Table 3
Sensitivity of the computed input impedance at 3500 MHz to the segmentation of the wire sections.

Segments per section	Total segments	Δ (mm)	$\frac{\Delta}{a}$	Z at 3500 MHz (Ω)	SWR
10 (used here)	1329	0.70	1.40	262.8 - j153.2	7.09
6	797	1.17	2.33	244.5 - j119.7	6.10
4	531	1.75	3.50	246.3 - j104.8	5.85
3	398	2.34	4.67	250.7 - j97.9	5.81
2	265	3.51	7.02	273.0 - j77.0	5.91

4.1.2. Excitation and feeding arrangement

The structure is excited by a delta-gap voltage source applied to a single segment located at the lower vertex of the layout, in the gap between the two innermost points of the bottom lobe. This idealised source imposes a perfectly balanced excitation and neglects the physical dimensions of the feed region, which is standard practice in NEC-2 modelling and adequate for comparative impedance studies.

A practical realisation would be fed by a 50 Ω coaxial line. Since the proposed layout is a balanced planar structure, connecting it directly to an unbalanced coaxial feed would allow currents to flow on the outer conductor of the cable, distorting the radiation pattern and shifting the measured input impedance away from the simulated value. A balun is therefore required. For a printed-circuit implementation a compact printed Marchand balun is the natural choice, as it can be etched on the same substrate as the radiator and integrated with the matching network; for a discrete-wire prototype a sleeve balun would be simpler to assemble. The insertion loss and residual imbalance introduced by the balun are not included in the results reported below, and are expected to be the dominant source of discrepancy between simulation and measurement.

4.2. Simulation without impedance matching

The antenna was first simulated at 3500 MHz, and then over the frequency range from 3400 MHz to 3600 MHz, which is the operating band proposed for fifth-generation (5G) cellular systems and the band for which this antenna is intended. Figure 9 summarizes the most relevant results of this first simulation:

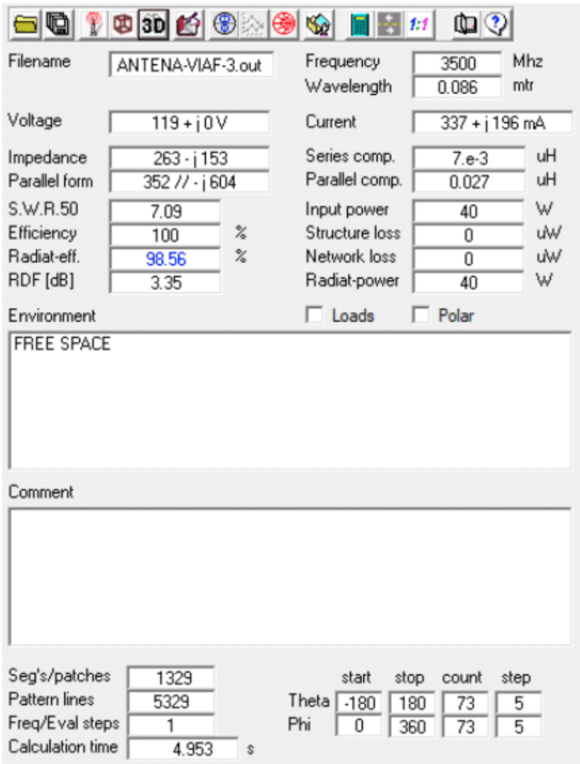

Figure 9: Main simulation parameters of the unmatched antenna at 3500 MHz.

- Input impedance $Z = 263 - j153\Omega$: a clear mismatch with respect to the 50 Ω reference of the coaxial cables used in radio communications.
- Standing wave ratio SWR = 7.09: this parameter measures the degree of impedance matching; ideally it should approach unity, and values between 1 and 1.6 are considered acceptable. In this unmatched condition a correspondingly large fraction of the incident power would be reflected at a 50 Ω generator.
- Radiation efficiency of 100%: the conductor is modelled as a perfect electric conductor, so the solver reports zero structure loss; this figure reflects the absence of ohmic loss in the model rather than a property of a physical prototype.
- Far-field integration accuracy of 98.56%: the power obtained by integrating the computed radiation pattern differs from the input power by 1.44%, which bounds the numerical accuracy of the pattern calculation. Note that the mismatch does not enter this figure, since the solver drives the antenna terminals directly; recovering the power that an SWR of 7.09 would reflect is precisely the purpose of the matching network of Section 4.3.

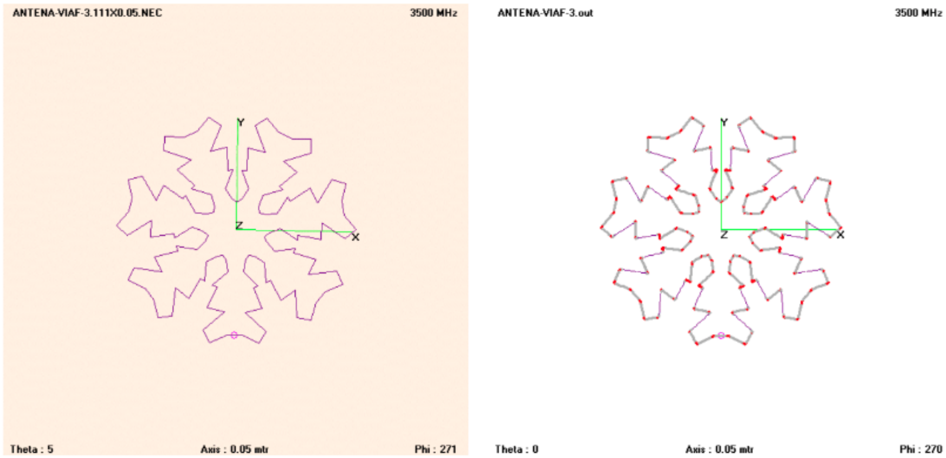

Figure 10: Antenna model (left) and radiating section (right).

Figures 11 and 12 show the horizontal and vertical radiation planes and the 3D radiation pattern. A sectorial radiation behavior is observed, with a maximum gain of 3.29 dBi, which makes the antenna well suited for 5G cellular base station applications.

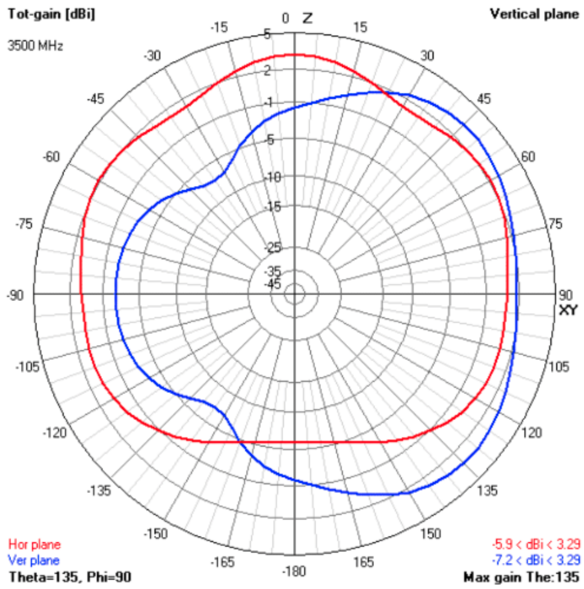

Figure 11: Horizontal and vertical radiation planes of the antenna.

The simulation was then extended to the range from 2400 MHz to 3700 MHz, beyond the 5G operating band of 3400–3600 MHz, in order to observe the antenna behavior outside this band and determine its potential operating range. As shown in Figure 13, the SWR remains between 6 and 10 across the sweep, which is inadmissible for practical use and is due to the mismatch of the antenna with respect to standard 50 Ω radio communication cables.

4.3. Impedance matching network

Next, the antenna was simulated with a radio-frequency impedance matching circuit of the high-pass type, as proposed by the 4NEC2 software. Figure 14 shows the resulting matching circuit: an L-type network based on a high-pass topology whose component values are a series capacitance of 0.37 pF and a shunt inductance of 5.27 nH.

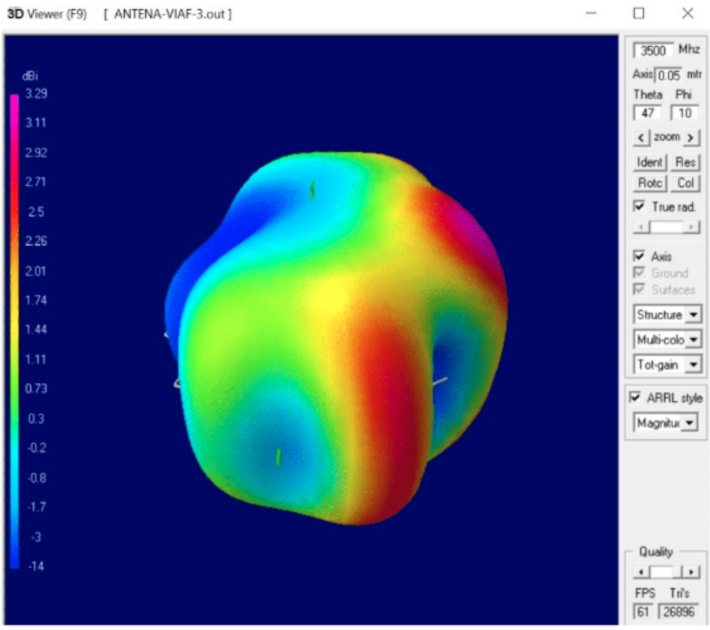

Figure 12: 3D radiation pattern of the antenna (maximum gain 3.29 dBi).

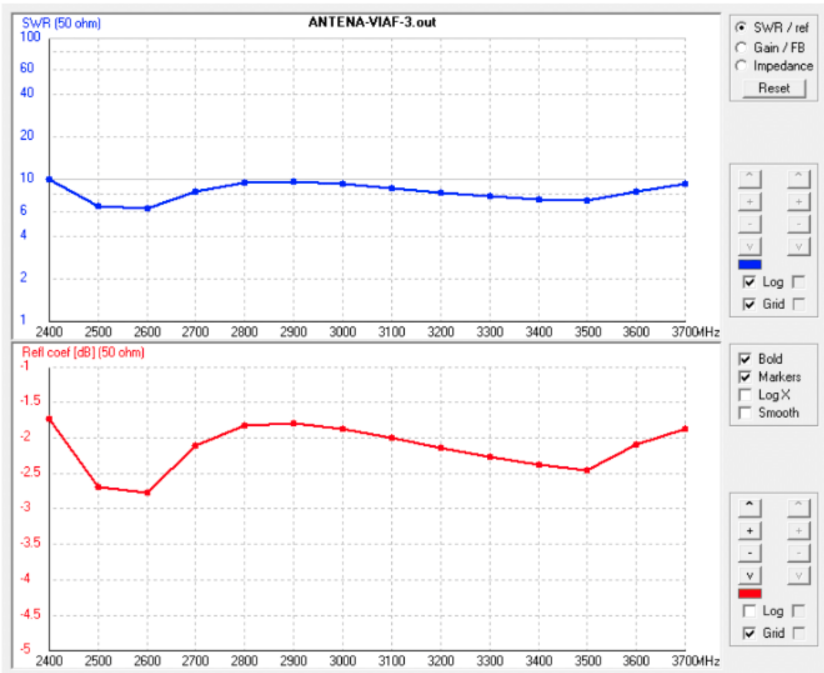

Figure 13: SWR and reflection coefficient of the unmatched antenna, frequency sweep from 2400 MHz to 3700 MHz.

4.4. Matched performance from 2400 MHz to 3700 MHz

Table 4 summarizes the SWR and the reflection coefficient Γ_{11} obtained with the matching network at six representative frequencies spanning the usable band, and Figure 15 gives the continuous swept response. Both are computed with the reactances of the two components evaluated at each frequency of the sweep, so that they describe a network that can actually be built.

Within the 3400-3600 MHz design band the matched antenna achieves SWR values between 1.003 and 1.276, with reflection coefficients below -18 dB and a best point of -56.7 dB at the design frequency. Away from the design frequency the match degrades as the two fixed components can no longer track

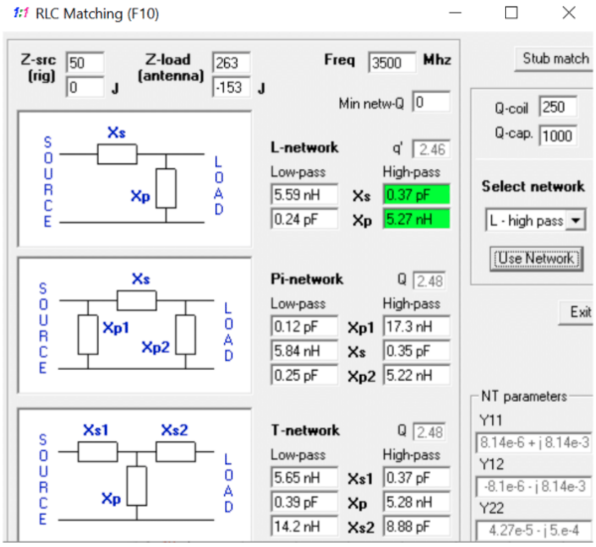

Figure 14: High-pass L-type impedance matching network for the 2400–3700 MHz range (Cs = 0.37 pF, Lp = 5.27 nH).

Table 4
SWR and reflection coefficient Γ_{11} of the matched antenna at representative frequencies.

Frequency (MHz)	**SWR**	Γ_{11} **(dB)**
3200	1.599	-12.8
3300	1.299	-17.7
3400	1.096	-6.8
3500	1.003	-56.7
3600	1.276	-18.3
3625	1.433	-15.0

the frequency variation of the antenna impedance: with physically realisable, dispersive components the criterion SWR $\leq$ 1.6 is met from approximately 3200 MHz to 3625 MHz, a 12.5% impedance bandwidth that covers the whole of the 3400-3600 MHz design band with a single radiating element and two lumped components. We stress that this figure must be obtained with the reactances of the capacitor and the inductor evaluated at each frequency of the sweep. Representing the network by a two-port whose parameters are computed once at the design frequency and then held constant, as some solver front-ends do by default, describes a non-dispersive network that no physical component realises, and overstates the achievable bandwidth substantially. Figure 15 also shows a second, narrower matched region between 3875 MHz and 3950 MHz, where the SWR returns to 1.38. This is the signature of the multi-resonant behaviour discussed in Section 3.1: the same fixed network re-matches the element at a neighbouring natural resonance of the 10.85 λ wire. Under the -6 dB criterion used in [3] the two regions merge and the response spans 3050-4050 MHz.

4.5. Cross-validation with a three-dimensional full-wave solver

NEC-2 represents the radiator as a set of thin, circular-section wires in free space and solves an electric-field integral equation by the method of moments. To bound the confidence that can be placed in this idealisation, the same geometry was re-analysed with an independent three-dimensional full-wave solver based on the finite integration technique [14]. In that model the radiator is a perfectly conducting rectangular strip 1.5 mm wide and 0.5 mm thick, with overall dimensions of 107 mm × 104 mm, excited

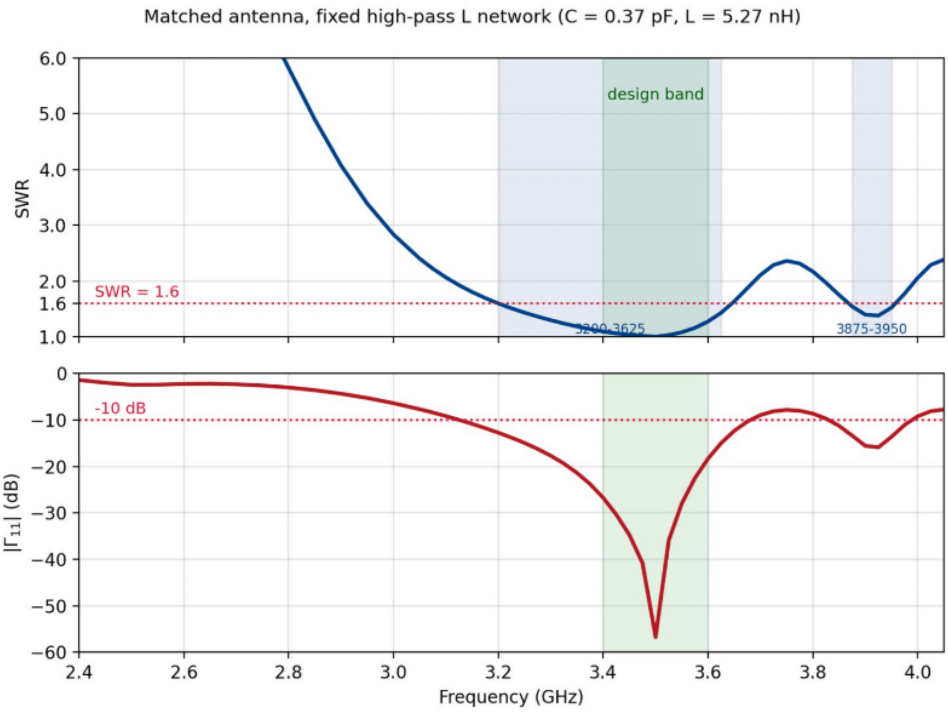

Figure 15: SWR and Γ_{11} of the matched antenna across the full sweep, computed with the reactances of the 0.37 pF capacitor and the 5.27 nH inductor evaluated at each frequency. The shaded region is the 3400–3600 MHz design band; the criterion SWR $\leq$ 1.6 is met from 3200 MHz to 3625 MHz.

by a discrete 50 Ω port at the lower gap of the layout. The transient solver was run from 2 to 4 GHz with no matching network, so that the comparison bears on the intrinsic behaviour of the radiator.

Table 5 compares the two models. The agreement is qualitative rather than numerical, and this is the expected outcome: the two solvers discretise different objects. NEC-2 sees a circular wire, the full-wave model a finite-thickness strip, and the equivalence between them is only approximate - a strip of width w behaves roughly like a wire of radius $\frac{w}{4}$ - while the full-wave model additionally includes a physical port of finite extent.

Table 5
Comparison between the NEC-2 wire model and the three-dimensional full-wave model.

Quantity	4NEC2 (NEC-2, MoM, wire)	Full-wave solver (FIT, strip)
Conductor model	circular wire, $a = 0.5$ mm	PEC strip, 1.5 mm × 0.5 mm
Overall dimensions	103 mm × 100 mm	107 mm × 104 mm
Excitation	delta-gap voltage source	discrete 50 Ω port
Simulated span	2400–3700 MHz	2000–4000 MHz
Frequency of best natural match	3500 MHz	3582 MHz (+2.3 %)
$\lvert\Gamma_{11}\rvert$ at that frequency, unmatched	-2.47 dB	-3.69 dB
SWR at 3500 MHz, unmatched	7.09	5.00
Peak gain / directivity	3.29 dBi (gain)	2.27 dBi (directivity)

Three points of agreement are decisive for the argument of this paper. First, both solvers find the unmatched element to be strongly mismatched to 50 Ω throughout the band, so that a matching network is not optional but structural. Second, both place the best natural match inside the n78 band, at 3500 MHz and 3582 MHz respectively, a discrepancy of 2.3%. Third, both return a reflection coefficient that varies smoothly and shallowly with frequency: over 2–4 GHz the full-wave model gives $\lvert\Gamma_{11}\rvert$

between 0.89 and 0.65 with no sharp resonance. It is this slow variation, itself a consequence of the many overlapping resonances of a developed wire length of the order of eleven wavelengths (Section 3.1), that allows a two-component network to hold a match over a comparatively wide span.

The residual quantitative differences — an unmatched SWR of 5.00 against 7.09 at 3500 MHz, and a directivity of 2.27 dBi against a computed gain of 3.29 dBi - are consistent with the wider effective conductor of the strip model. We therefore treat the NEC-2 results as reliable for the trends, the resonant behaviour and the radiation pattern, while noting that absolute impedance values, and hence the exact component values of the matching network, should be taken from the full-wave model before a prototype is built.

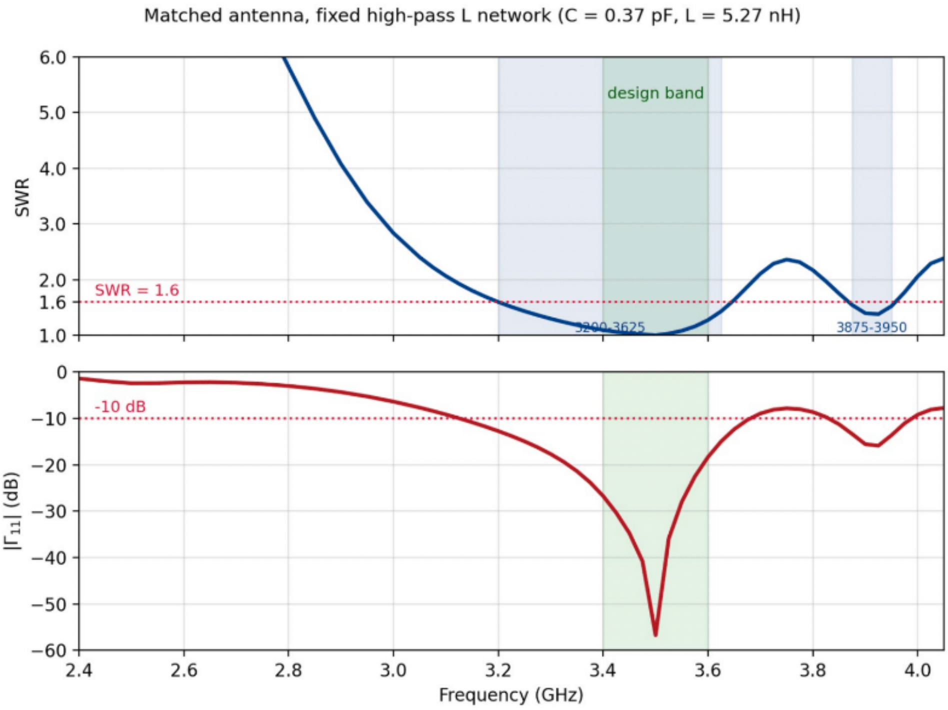

Figure 16: $|S11|$ of the unmatched element computed with the three-dimensional full-wave solver, referred to 50 Ω.

5. Discussion

The results indicate that geometry generation from curves on a lemniscatic torus is a viable alternative to conventional trial-and-error antenna shaping. Table 6 places the proposed element beside recently reported sub-6 GHz designs.

Table 6
Comparison with recently reported sub-6 GHz designs. n.r.: not reported in the source.

Ref.	Geometry	Band (GHz) and criterion	BW (%)	Ports	Footprint (mm)	Gain (dBi)	Feed and matching
[3]	π-shaped monopoles on a 16-sided polygon	3.3-6.0, at -6 dB	58	16	140 × 140, FR-4	n.r.	50 Ω microstrip; slotted ground for decoupling
[4]	flower-shaped monopole MIMO	2.88-6.12	72	4	54 × 54, FR-4	5.25	50 Ω microstrip; orthogonal elements for isolation
[5]	review of massive-MIMO arrays	sub-6 GHz	-	-	-	-	-
This work	lemniscatic-torus wire	3.20–3.63, at SWR ≤ 1.6 (-13 dB)	12.5	1	103 × 100, free-standing	3.29	two lumped components.

Two cautions are needed before reading the table. The first is that the matching criterion differs between the works compared: the 3.3-6.0 GHz figure of [3] is quoted at -6 dB, that is at an SWR of about 3, whereas the band reported here is quoted at SWR ≤ 1.6, equivalent to -13 dB. Applying the -6 dB criterion of [3] to the present element widens its band to 3050-4050 MHz, a fractional bandwidth of 28.2% rather than 12.5%. The comparison of fractional bandwidths in the table is therefore conservative towards our design. The second caution is that [3] does not report a gain figure, so that column cannot be completed for it.

With that said, the comparison must be read along the right axis. In raw bandwidth the proposed element does not lead: the multi-element configurations of [3] and [4] span considerably wider ranges even after the criteria are harmonised. What distinguishes the present design is the cost at which its bandwidth is obtained. The sixteen-port arrangement of [3] and the four-element configuration of [4] require feed networks, isolation structures and decoupling measures whose complexity grows with the element count — [3] shapes its ground plane with sixteen rectangular slots for that purpose, and [4] relies on an orthogonal placement of its four radiators — whereas the element proposed here is a single radiator with a single port matched by two lumped components. It is also the only one of the three that is not printed on FR-4, which leaves the substrate as a free design variable rather than a fixed constraint. The 3.29 dBi gain and sectorial pattern are consistent with the requirements of base-station panel elements discussed in [5].

The 3.29 dBi peak gain is nevertheless modest by comparison with the 8–10 dBi usually expected of an individual element in a base-station panel. This is the expected behaviour of a free-standing planar radiator with a bidirectional pattern, and it is not intrinsic to the geometry: placing the element approximately a quarter-wavelength — some 21 mm at 3.5 GHz — above a conducting reflector would suppress the rear lobe and is expected to raise the realised gain into the 7–9 dBi range while roughly halving the beamwidth. The reflector also perturbs the input impedance and would require the matching network to be recomputed.

5.1. Considerations for a printed-circuit realisation

The planar character of the layout makes a printed-circuit realisation the natural route to a prototype, but three effects that the free-space wire model omits would have to be accounted for. The first is the substrate. Etching the same geometry on a dielectric lowers its resonances by roughly the inverse square root of the effective permittivity; for a thin substrate with air above the trace, $\frac{\epsilon_{eff} \approx (\epsilon_r+1)}{2}$, so that on standard FR-4 ($\epsilon_r \approx 4.3$) the element would resonate near 2.1 GHz rather than 3.5 GHz, and its linear dimensions would have to be scaled by about 0.61 - to roughly 64 mm × 64 mm - to restore the design band. This is a welcome side effect, since it makes the element markedly more compact, but the rescaling must be re-optimised in a full-wave solver rather than applied blindly. The second is dielectric loss: FR-4 exhibits tan $\delta \approx 0.02$ at 3.5 GHz against 0.0027 for a microwave laminate such as RO4003C, a difference that translates directly into radiation efficiency and must be weighed against the substantially lower cost of FR-4 in an application whose premise is low-cost replication. The third is manufacturing tolerance: a typical etching tolerance of ± 0.1 mm represents about $\pm 7\%$ of the 1.5 mm trace width assumed in the full-wave model, and its effect on the input impedance should be quantified before committing to a production run. Conductor loss, by contrast, is not a concern: the skin depth in copper at 3.5 GHz is approximately 1.1 μm, well below the 35 μm thickness of standard 1 oz cladding.

The matching network was modelled with ideal lumped elements, and its physical realisation at 3.5 GHz deserves comment. A series capacitance of 0.37 pF is not a standard E24 value, and at sub-picofarad levels the absolute tolerance of commercial components is comparable to the value itself. More critically, the parasitic shunt capacitance of the mounting pads of an 0402 package is typically 0.1–0.2 pF, of the same order as the series element it would implement, while a 5.27 nH inductor in that package has a self-resonant frequency uncomfortably close to the operating band. A lumped implementation would therefore require careful de-embedding and would remain sensitive to assembly variation. A distributed equivalent is preferable: on a 0.813 mm RO4003C substrate the guided wavelength at 3.5 GHz is approximately 53 mm, so a series line section together with an open-circuited shunt stub of a few millimetres in length would implement the same transformation with etching tolerances only, at no additional component cost and with no parasitics to de-embed [18].

Several limitations should be stated plainly. The impedance results rest on wire-segment simulations cross-validated against a full-wave model that agrees on trends but not on absolute values, and neither model includes a dielectric substrate, a feeding connector, a balun or fabrication tolerances. The matching network is modelled with ideal lumped components whose practical realisation at 3.5 GHz is problematic for the reasons given above. No measurements have been performed, so every figure reported here is a simulated quantity. Future work will address, in order: the design of a printed Marchand balun and a distributed matching network; the fabrication of a PCB prototype on both FR-4 and a microwave laminate; experimental validation of the input impedance with a vector network analyser under SOLT calibration, and of the gain and radiation patterns in an anechoic chamber by comparison against a standard-gain horn; a systematic exploration of the parameter pairs (p, q) of Section 3.1 as a route to tailoring bandwidth and pattern; and the arrangement of several elements, with a reflector, into a base-station panel.

6. Conclusion

The mathematical analysis showed that there are infinitely many possibilities for selecting control points belonging to a curve that lies on a lemniscatic torus and is projected onto the plane. The control points that determine the antenna were computed symbolically and entered into the 4NEC2 software for simulation and analysis.

The impedance matching of the antenna was achieved with an LC network of the high-pass L type, consisting of a 0.37 pF capacitor and a 5.27 nH inductor. The simulations showed that the matched antenna has excellent performance in terms of SWR and $\Gamma_1 1$ to operate satisfactorily in the 5G mobile telephony band from 3400 MHz to 3600 MHz.

Beyond the design band the element retains a usable match over approximately 3200 MHz to 3625 MHz, a 12.5% impedance bandwidth, with two fixed components. We stress that all results reported here are simulated: the design is competitive in simulation, and its experimental validation remains to be carried out. Its principal merit at this stage is methodological — the geometry is derived in closed form, is completely specified by two coprime integers, and can be regenerated exactly by any reader from the expressions given in Sections 2 and 3.

Acknowledgements

This paper reports and extends results originally obtained in the undergraduate thesis of L. E. Román Pintado at Universidad Nacional de Piura [9], defended in April 2025 under the supervision of C. E. Arellano-Ramírez and R. Velezmoro-León. The choice-of-parameters analysis of Section 3.1, the full-wave cross-validation of Section 4.5 and the printed-circuit analysis of Section 5.1 are new to the present work.

Data and code availability

The complete list of 133 control points, the Mathematica notebook that generates the lemniscatic torus, the projected curve and the control points, and the 4NEC2 input file used for all simulations reported here are openly available at https://doi.org/10.5281/zenodo.21968529.

Declaration on Generative AI

During the preparation of this work, the authors used Claude (Anthropic) in order to check the grammar and improve the wording of the English text, and to assist with the numerical verification reported in

Sections 3.1, 4.1.1 and 4.4: the re-execution of the NEC-2 model, the segmentation study of Table 3 and the analysis of the matching network across frequency. The tool was not used to generate the antenna geometry, the simulations of Sections 4.1 to 4.4 or the full-wave model of Section 4.5, which are the authors' own work. After using this tool, the authors reviewed and edited the content as needed and take full responsibility for the publication's content.

References

[1] C. A. Balanis, et al., Antenna theory, volume 2, John wiley New York, 1982.

[2] J. López, I. Díaz, A. Sevilla, Introducción al análisis y diseño de antenas, Revista de la Escuela de Física 2 (2014) 82–98.

[3] T. G. Abouelnaga, I. Zewail, M. Shokair, 16-ports indoor base station mimo array for sub-6 ghz 5g applications, Telecommunication Systems 80 (2022) 589–597.

[4] T. Addepalli, R. Manda, M. A. Kumar, Monopole based flower-shaped 4-element mimo antenna with high diversity performance for 4g: Lte, 5g: sub-6 ghz (n77/n78/n79), wifi-5 and wifi-6 bands applications, Analog Integrated Circuits and Signal Processing 122 (2025) 5.

[5] S. K. Ibrahim, M. J. Singh, S. S. Al-Bawri, H. H. Ibrahim, M. T. Islam, M. S. Islam, A. Alzamil, W. M. Abdulkawi, Design, challenges and developments for 5g massive mimo antenna systems at sub 6-ghz band: a review, Nanomaterials 13 (2023) 520.

[6] A. Iglesias, R. Velesmoro, R. Ipanaque, Symbolic computational approach to construct a 3d torus via curvature, 2013.

[7] O. Shobayo, O. Abayomi-Alli, M. Odusami, S. Misra, M. Safiriyu, Modeling and simulation of impedance-based algorithm on overhead power distribution network using matlab, in: Advances in Electrical and Computer Technologies: Select Proceedings of ICAECT 2019, Springer, 2020, pp. 335–345.

[8] R. Velezmoro-León, C. E. Arellano-Ramírez, D. A. Flores-Córdova, R. Ipanaqué-Chero, Using mathematica and 4nec2 to design and simulation of an antenna in 2100 and 3500 mhz bands, in: International Conference on Computational Science and Its Applications, Springer, 2021, pp. 157–171.

[9] L. E. Román Pintado, Diseño y simulación de una antena obtenida a través de puntos de control de una curva proyectada de un toro lemniscático para aplicaciones 5G, 2025.

[10] S. Wolfram, An elementary introduction to the wolfram language, (No Title) (2015).

[11] S. Wolfram, The mathematica book, Wolfram Research, Inc., 2003.

[12] A. Voors, 4NEC2: NEC-based antenna modeler and optimizer, Online, 2021. URL: https://www.qsl.net/4nec2/, accessed: Aug. 5, 2026.

[13] G. J. Burke, A. J. Poggio, Numerical electromagnetics code (nec)-method of moments, 1981.

[14] Dassault Systèmes, CST studio suite 2025, 2025. URL: https://www.3ds.com/products/simulia/cst-studio-suite.

[15] M. P. Do Carmo, Differential geometry of curves and surfaces: revised and updated second edition, Courier Dover Publications, 2016.

[16] E. Abbena, S. Salamon, A. Gray, Modern differential geometry of curves and surfaces with Mathematica, CRC press, 2017.

[17] E. Weisstein, Run. mathworld-a wolfram web resource, Mathworld–A Wolfram Web Resource (2019).

[18] D. M. Pozar, et al., Microwave engineering, volume 3, wiley New York, 2005.